Research Square

Preprints are preliminary reports that have not undergone peer review.
They should not be considered conclusive, used to inform clinical practice,
or referenced by the media as validated information.

Annexin A2 Mediates Bevacizumab Resistance and Infiltrative Escape in Glioblastoma

ListTaketo Ezaki
Keio University School of Medicine
Ryota Tamura
Keio University School of Medicine
Yohei Yamamoto
The Jikei University School of Medicine
Jun Takei
The Jikei University School of Medicine
Akihiko Teshigawara
The Jikei University School of Medicine
Kyoichi Tomoto
The Jikei University School of Medicine
Yasuharu Akasaki
The Jikei University School of Medicine
Yuichi Murayama
The Jikei University School of Medicine
Masahiro Toda
Keio University School of Medicine
Hikaru Sasaki
Keio University School of Medicine
Keisuke Miyake
Kagawa University School of Medicine
Toshihide Tanaka
ttanaka123066@gmail.com

The Jikei University School of Medicine

Research Article

Keywords: Annexin A2, neoadjuvant Bevacizumab, glioblastoma, infiltrative escape

Posted Date: June 28th, 2026

DOI: https://doi.org/10.21203/rs.3.rs-10073018/v1

License: This work is licensed under a Creative Commons Attribution 4.0 International License.
Read Full License

Additional Declarations: No competing interests reported.

Version of Record: A version of this preprint was published at Journal of Neuro-Oncology on September 3rd, 2026. See the published version at https://doi.org/10.1007/s11060-026-05772-4.

Abstract

Purpose

The clinical benefit of bevacizumab (Bev) in glioblastoma (GBM) is typically transient, as tumors develop adaptive resistance characterized by an infiltrative shift from angiogenesis dependent growth. This study investigated Annexin A2 (ANXA2), a regulator of both angiogenesis and invasion, as a potential mediator of Bev resistance.

Methods

We analyzed 66 tissue-specimens from 33 GBM patients using quantitative real-time PCR and immunohistochemistry/immunofluorescence. The cohort included 15 Bev-naïve cases and 18 neoadjuvant Bev (neoBev) cases. 33 refractory specimens-including unique paired samples from the same patients at different treatment phases (initial resection vs. refractory stage) were evaluated to correlate ANXA2 expression levels with progression-free survival (PFS), overall survival (OS), and MRI recurrence patterns.

Results

Multivariate analysis identified high ANXA2 expression as a significant independent poor prognostic factor for both PFS and OS. In the neoBev group, patients with low ANXA2 mRNA expression levels demonstrated significantly superior survival outcome compared to those with high expression. While ANXA2 mRNA levels tended to increase at the refractory stage, a significant negative correlation was observed between the number of Bev cycles and ANXA2 expression levels. Histopathological analyses revealed intense ANXA2 expression in the vascular endothelial cells and stroma at the GBM leading edge, co-localization with the hypoxia marker hypoxia-inducible factor-1α.

Conclusions

ANXA2 is a key mediator of the adaptive transition from an angiogenic to infiltrative phenotype with Bev therapy. These findings suggest that ANXA2 serves as a robust predictive biomarker for Bev clinical benefit, and represents a promising therapeutic target for overcoming adaptive resistance in GBM.

Introduction

Glioblastoma (GBM) is the most malignant type of brain tumor, characterized by rapid progression and poor prognosis [1]. Bevacizumab (Bev) is approved as a standard treatment for GBM, particularly at recurrence. However, phase 3 trials have shown that Bev does not significantly improve overall survival

(OS) in primary GBM. Despite resulting in substantial tumor volume reduction, its therapeutic effects are transient [2, 3].

Reflecting Japan's unique approval of Bev for newly diagnosed GBM, we have previously investigated resistance mechanisms- including vascular endothelial growth factor (VEGF), tumor oxygenation, stemness, and immunoregulatory profiles- using paired surgical and autopsy specimens from patients naïve to, treated with, and refractory to Bev [4–10]. While Bev can effectively suppress angiogenesis, it may paradoxically promote tumor invasion, limiting long-term efficacy. Matrix metalloproteinases (MMPs), particularly MMP2 and MMP9, have been identified as prognostic indicators following Bev therapy, with elevated expression levels correlating with worse survival outcomes, suggesting a mechanistic link between anti-angiogenic treatment and invasive escape [11, 12]. Radiological studies have shown that recurrence patterns, specifically contrast-enhanced T1-weighted image with gadolinium contrast (T1-Gd) lesions versus T2 diffuse infiltration, are associated with different survival outcomes [13].

In GBM biology, angiogenesis and invasion operate as complementary processes [14]; consequently, prolonged bevacizumab exposure inevitably triggers a compensatory phenotypic shift from angiogenesis-dependent growth toward infiltrative escape [15, 16]. Elucidating the molecular drivers governing both modalities is therefore paramount to understanding adaptive resistance. Annexin A2 (ANXA2) is frequently overexpressed and has been associated with increased invasiveness, epithelial-mesenchymal transition (EMT), and poor clinical outcomes in GBM [17, 18] Functionally, ANXA2 facilitates extracellular matrix degradation by activating plasminogen and downstream MMP2 and MMP9, known contributors to GBM invasion [19, 20]. Given its dual role of upstream regulation in both angiogenesis and invasion, we hypothesized that ANXA2 is potentially a more reliable predictive biomarker than well-known invasion molecules, including MMP2, MMP9, tissue inhibitor of metalloproteinase (TIMP-1), and plasminogen activator inhibitor (PAI-1) [21, 22], and underlie the observed adaptive resistance to Bev in GBM.

We utilize a globally unique cohort of neoadjuvant Bev-treated (neoBev) and paired longitudinal specimens to clarify how ANXA2-mediated invasiveness drives Bev resistance and dictates clinical outcomes.

Materials and Methods

Patient eligibility and sample collection

This study used 66 GBM tissues from 33 patients obtained from three different settings: 18 resected after neoBev administration (during Bev response; neoBev group), 15 newly diagnosed GBM without any previous treatment (naïve Bev group), and 33 recurrent GBM after Bev administration (refractory Bev group). The refractory Bev group included 22 autopsy and 11 salvage surgery speciments (Fig. 1). Patient selection was conducted in accordance with the inclusion and exclusion criteria of a previous

phase II study [8]. As paired specimens from the same patient, 29 naïve-refractory Bev specimens from 15 cases (including 11 autopsy and four salvage surgery) and 18 neoBev-refractory Bev specimens from 18 cases (including 11 autopsy and seven salvage surgery) were obtained. The baseline characteristics and treatment profiles of the patients are shown in Table 1 and **Supplementary TableS1**.

Table 1 Baseline characteristic of patients

Treatment protocol

All neoBev patients were treated with preoperative neoBev at 10 mg/kg on day 0. Surgical resection was performed 3 to 4 weeks after neoBev administration. Maintenance treatment with temozolomide (TMZ) began 4 weeks after the completion of radiotherapy at a starting dose of 150 mg/m^2 for five consecutive days of a 28-day cycle. All newly diagnosed GBM patients (naïve Bev) were treated with a concomitant Stupp regimen and Bev at 10 mg/kg every two weeks after surgical resection [9, 10].

Study oversight

The study protocol was approved by the institutional review boards of Keio University School of Medicine (N20050002), The Jikei University School of Medicine (JKI 018–052), and Kagawa University School of Medicine (2018KH046), and conducted in accordance with the Declaration of Helsinki. Written informed consent was obtained from all participants.

RNA extraction, complementary DNA (cDNA) synthesis, and quantitative real-time PCR (qRT-PCR)

Total RNA was extracted from formalin-fixed paraffin-embedded (FFPE) tissue samples using the NucleoSpin totalRNA FFPE kit (Takara Bio Inc., Shiga, Japan) and quantified with a NanoDrop Lite Plus spectrophotometer (Thermo Fisher Scientific K.K., Tokyo, Japan). Because of the fragmented nature of RNA derived from FFPE samples, RNA quality was not evaluated by RNA integrity number. Instead, glyceraldehyde 3-phosphate dehydrogenase (GAPDH) and beta-actin (ACTβ), commonly used housekeeping genes, were employed as internal controls to normalize gene expression levels in the qRT-PCR analysis. Next, cDNA was synthesized from total RNA using the PrimeScript™ II 1st Strand cDNA Synthesis Kit (Takara Bio Inc.) with a TaKaRa PCR Thermal Cycler (Takara Bio Inc.) following the manufacturer's protocol.

qRT-PCR was conducted using PowerUp™ SYBR™ Green Master Mix (Thermo Fisher Scientific K.K.) on an Applied Biosystems ViiA™ 7 Real-Time PCR System (Thermo Fisher Scientific K.K.). The thermal cycling conditions were as follows: 95°C for 2 minutes, followed by 40 cycles of 95°C for 15 s and 60°C for 1 minute. Gene expression levels were analyzed using the comparative cycle threshold (ΔCt) method. GAPDH and ACTβ were used as internal control genes to ensure robust normalization. Gene-specific

primers for ANXA2 were synthesized by Eurofins Genomics K.K. (Tokyo, Japan) [23] (**Supplementary TableS2)**. For each sample, Ct values for the target and internal control genes were determined. The ΔCt value was calculated as follows:

$$\Delta Ct = Ct_{\text{target gene}} - \frac{CtGAPDH + CtACT\beta}{2}$$

The relative expression level of ANXA2 was calculated using the $2^{-\Delta Ct}$ method.

For statistical analysis, the relative expression values were transformed into a base − 10 logarithmic scale as follows:

$$\log_{10}(2^{-\Delta Ct}) = -\Delta Ct \cdot \log_{10}(2)$$

Log-transformed expression values were used for all statistical analyses. ANXA2 expression levels were dichotomized into high and low groups relative to the median value.

Immunohistochemistry (IHC) and immunofluorescence (IF)

To evaluate ANXA2 protein expression, 3-μm FFPE tissue sections underwent microwave antigen retrieval in 10 mM citrate buffer (pH 6.0) [9]. After blocking with 2.5% normal horse serum (ImmPress Detection Systems, Vector Laboratories, Newark, CA, USA) for 1 hour at room temperature, sections were incubated overnight at 4°C with an anti-ANXA2 primary antibody (1:200, sc-28385, Santa Cruz Biotechnology, TX, USA). Immunostaining within the tumor core and leading-edge areas was evaluated at 400x magnification by three neurosurgeons and one neuropathologist [24].

For spatial distribution analysis, triple-label IF was performed for ANXA2, hypoxia-inducible factor (HIF)-1α, and CD133. Following blocking, sections were incubated overnight at 4°C with primary antibodies against ANXA2, HIF-1α (1:50, AF1935, R&D Systems, Minneapolis, MN, USA), and CD133 (1:50, 18470-1-AP, Proteintech, Rosemont, IL, USA). Signals were visualized using Alexa Fluor 555- (red), 488- (green), and 647-conjugated (far-red/magenta) secondary antibodies (ImmPRESS HRP KIT; Anti-MOUSE IgG for ANXA2, Anti-GOAT IgG for HIF-1α, Anti-RABBIT IgG; Vector Laboratories, CA, USA), with DAPI counterstaining for nuclei. Endogenous autofluorescence was mitigated using the Vector TrueView Autofluorescence Quenching Kit (SP-8500, Vector Laboratories) for 5 minutes. Confocal images were captured via sequential laser scanning (405/488/555/647 nm) to eliminate spectral crosstalk.

Recurrence magnetic resonance imaging (MRI) pattern and modified Response Assessment in Neuro-Oncology (RANO) 2.0

All patients were followed up regularly with MRI. The recurrence MRI pattern was classified into three settings: cT1-flare up, T2 diffuse, and T2 circumscribed [9, 13, 25]. The reduction rates (RR) of T1 and

T2/FLAIR were calculated and evaluated by neurosurgeons. The modified RANO 2.0 (mRANO 2.0) criteria were applied to assess radiological response in GBM patients, incorporating both contrast-enhancing (T1-Gd) and non-enhancing (FLAIR) MRI features, alongside clinical and steroidal parameters [26]. In this study, the clinical status and steroid dosage changes were assumed to be stable. The classification in the neoBev group is shown in **Supplementary TableS3**.

Statistical analyses

Baseline patient characteristics were compared using the Mann-Whitney U, Fisher's exact, or χ^2 tests. Progression-free survival (PFS) and OS were estimated via Kaplan- Meier analysis and compared using the log-rank test. Multivariable Cox proportional hazards regression models -adjusting for age, sex, extent of resection, and cumulative TMZ and Bev cycles- were employed to determine independent prognostic factors.

For paired continuous data from identical patients, ANXA2 expression levels were compared using the Wilcoxon signed-rank test. Correlations between cumulative Bev cycles and ANXA2 expression were evaluated using Spearman's rank correlation coefficient, with dose subgroups (0–10, 11–20, and ≥ 21) compared via the Kruskal-Wallis test. The Kruskal-Wallis test was also applied to analyze expression levels across recurrence MRI patterns. Missing survival data were handled by case-wise deletion. Statistical analyses and graphing were performed using GraphPad Prism 11 and IBM SPSS Statistics. Two-sided $P < 0.05$ was considered statistically significant. This study was not randomized.

Results

Patient characteristics

The patient characteristics are summarized in Table 1 and **Supplementary TableS1**. Multivariate Cox regression analysis showed that neoBev was independently associated with longer PFS (hazard ratio (HR): 0.33, $P = 0.010$), but not OS (**Supplementary TableS4**). Independent factors for OS included male sex ($P = 0.025$) and longer TMZ exposure ($P = 0.031$). Notably, high ANXA2 mRNA expression levels remained a robust independent prognostic factor for both shorter PFS (HR: 2.85, $P = 0.028$) and shorter OS (HR: 3.12, $P = 0.015$) (**Supplementary TableS4**).

Comparative analyses using paired samples

To validate the ANXA2 mRNA expression level results, paired samples obtained from naïve-refractory Bev and neoBev-refractory Bev cases were compared. No significant differences in ANXA2 mRNA expression levels were observed ($P = 0.244$ and 0.205, respectively), although both comparisons showed a trend toward increased expression levels in the refractory setting (Fig. 2a).

Dose-dependent ANXA2 mRNA expression changes with Bev treatment

Next, we performed linear regression analyses between the log-transformed ANXA2 mRNA expression levels and total number of Bev treatment cycles. Rather than separating the data into naïve and neoBev groups, all samples were analyzed as a single cohort. Notably, a significant negative correlation was found, with ANXA2 mRNA expression levels decreasing with increasing Bev exposure (r = -0.456, *P* = 0.009) (Fig. 2b).

To assess the impact of cumulative Bev administrations on the ANXA2 mRNA expression profiles, we stratified the patients by treatment cycle count into three groups (0–10, 11–20, ≥ 21 cycles). Then, log-transformed ANXA2 mRNA expression levels were observed when comparing the three groups, with expression significantly decreased in the 11–20 dose group compared with the ≤ 10 dose group (*P* = 0.017). Additionally, patients receiving more than 20 bevacizumab doses maintained lower ANXA2 mRNA expression levels compared with those receiving fewer doses (Fig. 2c).

IHC and IF analyses

ANXA2 protein expression levels in the tumor core and leading-edge area were evaluated by IHC staining of the tumor stroma. ANXA2 showed cytoplasmic expression in neoplastic glial cells and was also detected within the stromal compartment in the tumor core, with vascular endothelial cells demonstrating prominent cytoplasmic ANXA2 expression at the leading edge (Fig. 3a). Only a small subset of reactive astrocytes exhibited positive ANXA2 IHC staining. Representative single channel IF images of DAPI (nuclei; blue), HIF-1α (nuclear/cytoplasmic; green), ANXA2 (cytoplasmic with additional stromal signal; red), and CD133 (membranous/punctate; magenta) staining are shown (Fig. 3b), along with merged images from the tumor core and leading edge (Fig. 3c). Neither the IHC nor IF assays revealed notable differences in HIF-1α, ANXA2, and CD133 protein staining patterns between the naïve Bev and neoBev groups. However, HIF-1α protein expression was almost absent at the leading-edge area.

Molecular profiles vary across recurrence MRI patterns and mRANO 2.0 analysis

Within each MRI recurrence patterns (cT1-flare up, T2 circumscribed, and T2 diffuse), ANXA2 expression did not differ significantly between the naïve and neoBev groups (*P* = 0.911 and *P* = 0.882, respectively; **Supplementary Fig.S1a**). A total of 18 patients in the neoBev group were evaluated using the mRANO 2.0 criteria: four patients were classified as partial response, 13 as stable disease, and one as progressive disease (**Supplementary TableS3**). Kaplan-Meier analysis showed no statistically significant differences in PFS or OS among the three response groups (**Supplementary Fig.S1b**).

Survival outcomes and ANXA2 expression patterns

ANXA2 mRNA expression levels were dichotomized relative to the median value. No statistically significant difference in PFS was observed between the high- and low-ANXA2 expression groups (6.5 months vs. 7.5 months in naïve Bev and 6.7 months vs. 9.9 months in neoBev, respectively). However, OS was statistically significantly longer in the low-ANXA2 expression group (18.0 months vs. 21.8 months in naïve Bev and 10.9 months vs. 19.9 months in neoBev; *P* = 0.003) (**Supplementary Fig.S3, Supplementary TableS5**). A subgroup analysis of PFS revealed that although no significant difference was observed between the high-ANXA2 expression neoBev and naïve Bev subgroups, the naïve Bev high-ANXA2 expression group showed a trend toward longer PFS, with a subset of patients demonstrating prolonged PFS beyond the median. In contrast, among patients in the low-ANXA2 expression group, those treated with neoBev demonstrated significantly longer PFS compared with those in the naïve Bev group (*P* = 0.006). Furthermore, within the neoBev cohort, low ANXA2 expression was associated with significantly prolonged PFS compared with high expression (*P* = 0.034) (Fig. 4a). For OS, the neoBev high-ANXA2 expression group had significantly worse OS than the naïve Bev high-ANXA2 expression group (*P* **=** 0.029). In contrast, no significant difference in OS was observed between the low-ANXA2 expression groups in the naïve Bev and neoBev patient groups. Within the neoBev cohort, patients with low ANXA2 expression achieved significantly longer OS compared with those with high expression (*P* = 0.004). No significant difference in OS was observed between the naïve Bev high-ANXA2 expression group and neoBev low-ANXA2 expression group (Fig. 4b). Consistent with these findings, pairwise comparisons of HRs across the treatment and expression subgroups further clarified these prognostic differences (**Supplementary TableS6**). In a comprehensive analysis using the neoBev low-ANXA2 expression group as a benchmark, the neoBev high-ANXA2 expression group exhibited a markedly elevated risk of death (OS HR: 2.701, 95% confidence interval: 0.953–7.660, *P* = 0.061), whereas the risk profile of the naïve Bev groups were less pronounced relative to that of neoBev low-ANXA2 expression cohort (**Supplementary TableS7**).

Discussion

Leveraging a globally unique cohort of neoadjuvant bevacizumab-treated (neoBev) glioblastoma specimens exclusively available in Japan, this study provides novel insights into the molecular dynamics induced by anti-angiogenic therapy. Despite baseline clinical disadvantages in the neoBev cohort-including advanced age and limited treatment exposure- neoBev remained independently associated with prolonged PFS. Intriguingly, while bevacizumab treatment typically downregulates ANXA2, elevated expression persisted in a subset of neoBev patients, correlating with significantly compromised PFS and OS. These findings establish ANXA2 not merely as a prognostic indicator, but as a critical molecular driver of resistance-associated infiltrative escape.

ANXA2 regulates plasmin generation and activates downstream MMPs, such as MMP2 and MMP9, to promote angiogenesis and extracellular matrix degradation [27]. With Bev therapy, GBM may shift from angiogenesis-dependent growth toward an invasion-driven phenotype [28], a transition in which the ANXA2-plasmin-MMP axis is likely involved [14]. Its roles in neoangiogenesis and matrix remodeling further support this adaptive mechanism [29–33]. Furthermore, ANXA2 is directly regulated by HIF-1α

through a hypoxia-responsive element [34]. It can also stabilize HIF-1α, creating a positive feedback loop that supports tumor progression [33]. Additionally, the ANXA2-mediated signaling axis has been implicated in driving mesenchymal phenotypic changes and adaptive resistance to anti-angiogenic therapy in GBM [35]. Given that the phenotypic balance between angiogenesis and invasion determines the therapeutic efficacy of Bev, the present study highlights the critical importance of monitoring ANXA2 regulation under Bev treatment.

The dynamic changes in the angiogenic and invasive phenotypes of GBM during Bev therapy are shown in Fig. 5. ANXA2 plays a potentially pivotal role in regulating the angiogenesis/invasion dependency for tumor growth and Bev therapeutic efficacy in this cancer. In addition, ANXA2 contributes to glioma stemness and resistance to radiotherapy, acting as a central mediator of invasive adaptation under anti-VEGF treatment. Specifically, recent evidence indicates that lactylation-driven, ubiquitin-specific protease 4 mediated stabilization of ANXA2 promotes the maintenance and radioresistance of glioblastoma stem cells, thereby reinforcing the tumor's survival scaffold [21].

While our paired analysis showed an overall trend of upregulated ANXA2 expression levels at recurrence, we observed a dose-dependent inverse correlation between ANXA2 expression levels and the number of Bev cycles. This suggested that maintaining low ANXA2 expression levels, thereby avoiding HIF-1α/ANXA2 axis activation, reflects higher Bev sensitivity. Thus, Bev-induced hypoxia activates HIF-1α, which directly upregulates ANXA2 to drive an infiltrative phenotype, thereby dictating patient survival outcomes. Interestingly, high ANXA2 expression patterns may counteract the benefits of neoBev. Crucially, our data demonstrated that neoBev significantly improved PFS only in the low-ANXA2 expression subgroup. This observation was further supported by our multivariate analysis (**Supplementary TableS5**). Pairwise comparisons and comprehensive analysis using the neoBev low-ANXA2 expression cohort as a benchmark revealed a distinct survival hierarchy, with the neoBev high-ANXA2 expression group notably carrying a nearly 2.7-fold higher risk of death compared with the neoBev low-ANXA2 expression group (**Supplementary TablesS6 and S7**). This pronounced difference indicates that low ANXA2 expression is a prerequisite for neoBev to provide clinical benefits by maintaining anti-angiogenic sensitivity. These findings support implementing a clinical strategy of ANXA2-guided neoBev, where patients identified via biopsy as having low tumor ANXA2 expression levels would benefit most.

The radiological response assessed by mRANO 2.0 did not significantly correlate with survival, suggesting that the imaging-based response alone may not fully reflect the underlying biological aggressiveness with Bev therapy. In addition, the ANXA2 expression patterns did not significantly differ across MRI recurrence patterns in either the naïve Bev or neoBev group. Given that anti-angiogenic therapy can induce heterogeneous, infiltrative recurrence patterns that often elude conventional radiographic response criteria [9, 13, 25], ANXA2, through its regulation of the plasmin-MMP axis and extracellular matrix remodeling, may serve as a critical complementary molecular indicator of invasion-driven adaptation.

This retrospective study has limitations, including residual confounding factors such as TMZ exposure and sex. Therefore, the observed neoBev benefit should be interpreted primarily in terms of PFS, with OS requiring further validation. Additionally, the limited number of salvage surgical specimens may have reduced the statistical power of this work. In conclusion, dynamic changes in ANXA2 expression levels during Bev treatment can significantly influence patient outcomes. Reflecting Bev-induced changes, ANXA2 can mediate both angiogenesis and tumor invasion. These results identify ANXA2 as a versatile molecular indicator, serving as both a prognostic factor and a predictive biomarker for neoBev therapy.

Declarations

Conflict of interest

All authors declare no competing interests.

Authorship contributions

Conceptualization: Taketo Ezaki, Ryota Tamura, Hikaru Sasaki, Keisuke Miyake, Toshihide Tanaka.

Methodology and Design: Taketo Ezaki, Ryota Tamura, Hikaru Sasaki, Keisuke Miyake, Toshihide Tanaka.

Investigation and Formal Analysis: Taketo Ezaki, Ryota Tamura, Hikaru Sasaki, Keisuke Miyake, Toshihide Tanaka.

Provision of Clinical Samples: Yohei Yamamoto, Jun Takei, Akihiko Teshigawara, Kyoichi Tomoto, Yasuharu Akasaki, Keisuke Miyake., Yuichi Murayama, Toshihide Tanaka

Data Acquisition: Ryota Tamura, Yohei Yamamoto, Jun Takei, Toshihide Tanaka.

Pathological Assessment: Taketo Ezaki, Ryota Tamura, Hikaru Sasaki, Toshihide Tanaka.

Discussion and Manuscript Review: Ryota Tamura, Jun Takei, Masahiro Toda, Toshihide Tanaka.

Writing - Original Draft Preparation: Taketo Ezaki.

Writing - Review and Editing: All authors.

Ethics approval

This study was performed in line with the principles of the Declaration of Helsinki. This study was also conducted according to institutional and national regulations and was approved by each institutional ethics committee (approval number N20050002 for Keio, JKI 018–052 for Jikei, and 2018KH046 for Kagawa).

Consent to participate

Informed consent was obtained from all individual patients included in the study.

Consent to publish

The authors affirm that human research participants provided informed consent for publication of the images in all figures and tables.

Funding

This work was supported by Fukuzawa Fund (Keio Gijuku Fukuzawa Memorial Fund for the Advancement of Education and Research).

Author Contribution

T.E. and T.T. wrote the main manuscript text and E.T. prepared figures and table. R.T., Y.Y. , J.T., K.T., A.T., H.K., and K.M. provided the surgical samples for analyses.M.T., Y.A., and Y.Y. supervised the current research.All authors reviewed the manuscript.

Acknowledgement

The authors greatly thank Ms. Marina Minami at the Division of Diagnostic Pathology, The Jikei University School of Medicine Kashiwa Hospital, Ms. Eiko Kuhara at the Department of Neurosurgery, The Jikei University School of Medicine, and Ms. Yuko Aikawa at the Department of Neurosurgery, Keio University School of Medicine for technical assistance with laboratory work and sample preparation. We also thank J. Iacona, Ph.D., from Edanz (https://jp.edanz.com/ac) for editing a draft of this manuscript.

Data availability

The datasets generated and/or analyzed during the current study are available from the corresponding author on reasonable request.

References

1. Louis DN, Perry A, Wesseling P et al (2021) The 2021 WHO Classification of Tumors of the Central Nervous System: a summary. Neuro Oncol 23(8):1231–1251. 10.1093/neuonc/noab106. PMID: 34185076; PMCID: PMC8328013
2. Chinot OL, Wick W, Mason W et al (2014) Bevacizumab plus radiotherapy-temozolomide for newly diagnosed glioblastoma. N Engl J Med. ;370(8):709 – 22. 10.1056/NEJMoa1308345. PMID:

24552318

3. Gilbert MR, Dignam JJ, Armstrong TS et al (2014) A randomized trial of bevacizumab for newly diagnosed glioblastoma. N Engl J Med 370(8):699–708. 10.1056/NEJMoa1308573. PMID: 24552317; PMCID: PMC4201043
4. Tamura R, Tanaka T, Miyake K et al (2016) Histopathological investigation of glioblastomas resected under bevacizumab treatment. Oncotarget 7(32):52423–52435. 10.18632/oncotarget.9387. PMID: 27244880; PMCID: PMC5239563
5. Tamura R, Tanaka T, Ohara K et al (2019) Persistent restoration to the immunosupportive tumor microenvironment in glioblastoma by bevacizumab. Cancer Sci 110(2):499–508. 10.1111/cas.13889. Epub 2018 Dec 21. PMID: 30467920; PMCID: PMC6361613
6. Yamamoto Y, Tamura R, Tanaka T et al (2017) Paradoxical findings of tumor vascularity and oxygenation in recurrent glioblastomas refractory to bevacizumab. Oncotarget 8(61):103890–103899. 10.18632/oncotarget.21978. PMID: 29262608; PMCID: PMC5732774
7. Takei J, Fukasawa N, Tanaka T et al (2022) Impact of Neoadjuvant Bevacizumab on Neuroradiographic Response and Histological Findings Related to Tumor Stemness and the Hypoxic Tumor Microenvironment in Glioblastoma: Paired Comparison Between Newly Diagnosed and Recurrent Glioblastomas. Front Oncol 12:898614 PMID: 35785200; PMCID: PMC9247463
8. Tanaka T, Tamura R, Takei J et al (2024) An exploratory prospective phase II study of preoperative neoadjuvant bevacizumab and temozolomide for newly diagnosed glioblastoma. J Neurooncol 166(3):557–567. 10.1007/s11060-023-04544-8. Epub 2024 Jan 31. PMID: 38291182; PMCID: PMC10876816
9. Ezaki T, Tanaka T, Tamura R et al (2024) Status of alternative angiogenic pathways in glioblastoma resected under and after bevacizumab treatment. Brain Tumor Pathol. ;41(2):61–72. doi: 10.1007/s10014-024-00481-0. Epub 2024 Apr 15. Erratum in: Brain Tumor Pathol. 2024;41(3–4):155. 10.1007/s10014-024-00485-w. PMID: 38619734; PMCID: PMC11052834
10. Iwauchi A, Fukasawa N, Takei J et al (2024) Comparative analyses of erythroblast transformation specific-1 related gene expression before and after neoadjuvant bevacizumab therapy for newly diagnosed glioblastoma. Int J Clin Exp Pathol 17(10):346–359 PMID: 39544713; PMCID: PMC11558313
11. Tabouret E, Boudouresque F, Barrie M et al (2014) Association of matrix metalloproteinase 2 plasma level with response and survival in patients treated with bevacizumab for recurrent high-grade glioma. Neuro Oncol 16(3):392–399. 10.1093/neuonc/not226. Epub 2013 Dec 9. PMID: 24327581; PMCID: PMC3922517
12. Tabouret E, Boudouresque F, Farina P et al (2015) MMP2 and MMP9 as candidate biomarkers to monitor bevacizumab therapy in high-grade glioma. Neuro Oncol 17(8):1174–1176. 10.1093/neuonc/nov094. PMID: 26142442; PMCID: PMC4490881
13. Nowosielski M, Wiestler B, Goebel G et al (2014) Progression types after antiangiogenic therapy are related to outcome in recurrent glioblastoma. Neurology. ;82(19):1684-92.

10.1212/WNL.0000000000000402. Epub 2014 Apr 11. PMID: 24727314

14. Ichikawa T, Otani Y, Kurozumi K, Date I (2016) Phenotypic Transition as a Survival Strategy of Glioma. Neurol Med Chir (Tokyo) 56(7):387–395. 10.2176/nmc.ra.2016-0077. Epub 2016 May 11. PMID: 27169497; PMCID: PMC4945597
15. Yamasaki F, Kurisu K, Aoki T et al (2012) Advantages of high b-value diffusion-weighted imaging to diagnose pseudo-responses in patients with recurrent glioma after bevacizumab treatment. Eur J Radiol 81(10):2805–2810. 10.1016/j.ejrad.2011.10.018. Epub 2011 Nov 17. PMID: 22100373
16. Reardon DA, Turner S, Peters KB et al (2011) A review of VEGF/VEGFR-targeted therapeutics for recurrent glioblastoma. J Natl Compr Canc Netw 9(4):414–427. 10.6004/jnccn.2011.0038. PMID: 21464146; PMCID: PMC3399727
17. Bao S, Wu Q, McLendon RE et al (2006) Glioma stem cells promote radioresistance by preferential activation of the DNA damage response. Nature 444(7120):756–760. 10.1038/nature05236. Epub 2006 Oct 18. PMID: 17051156
18. Lokman NA, Ween MP, Oehler MK, Ricciardelli C (2011) The role of annexin A2 in tumorigenesis and cancer progression. Cancer Microenviron 4(2):199–208. 10.1007/s12307-011-0064-9. Epub 2011 Mar 5. PMID: 21909879; PMCID: PMC3170418
19. Tu Y, Xu L, Fu G et al (2025) Lactylation-driven USP4-mediated ANXA2 stabilization and activation promotes maintenance and radioresistance of glioblastoma stem cells. Cell Death Differ 32(9):1648–1663. 10.1038/s41418-025-01494-8. Epub 2025 Apr 4. PMID: 40185997; PMCID: PMC12432172
20. Liu W, Hajjar KA (2016) The annexin A2 system and angiogenesis. Biol Chem. ;397(10):1005-16. 10.1515/hsz-2016-0166. PMID: 27366903
21. Liu L, Yang S, Lin K, Yu X et al (2022) Sp1 induced gene TIMP1 is related to immune cell infiltration in glioblastoma. Sci Rep 12(1):11181. 10.1038/s41598-022-14751-4. PMID: 35778451; PMCID: PMC9249770
22. Seker F, Cingoz A, Sur-Erdem İ et al (2019) Identification of *SERPINE1* as a Regulator of Glioblastoma Cell Dispersal with Transcriptome Profiling. Cancers (Basel) 11(11):1651. 10.3390/cancers11111651. PMID: 31731490; PMCID: PMC6896086
23. Renner B, Tong HH, Laskowski J et al (2016) Annexin A2 Enhances Complement Activation by Inhibiting Factor H. J Immunol 196(3):1355–1365. 10.4049/jimmunol.1500793. Epub 2016 Jan 4. PMID: 26729803; PMCID: PMC4724541
24. Ezaki T, Sasaki H, Hirose Y et al (2011 Nov-Dec) Molecular characteristics of pediatric non-ependymal, non-pilocytic gliomas associated with resistance to temozolomide. Mol Med Rep 4(6):1101–1105. 10.3892/mmr.2011.573. Epub 2011 Aug 25. PMID: 21874248
25. DeLay M, Jahangiri A, Carbonell WS et al (2012) Microarray analysis verifies two distinct phenotypes of glioblastomas resistant to antiangiogenic therapy. Clin Cancer Res 18(10):2930–2942. 10.1158/1078-0432.CCR-11-2390. Epub 2012 Apr 3. PMID: 22472177; PMCID: PMC3354006

26. Wen PY, van den Bent M, Youssef G et al (2023) RANO 2.0: Update to the Response Assessment in Neuro-Oncology Criteria for High- and Low-Grade Gliomas in Adults. J Clin Oncol 41(33):5187–5199 Epub 2023 Sep 29. PMID: 37774317; PMCID: PMC10860967
27. Onishi M, Ichikawa T, Kurozumi K et al (2015) Annexin A2 regulates angiogenesis and invasion phenotypes of malignant glioma. Brain Tumor Pathol 32(3):184–194. 10.1007/s10014-015-0216-6. Epub 2015 Feb 20. PMID: 25697644
28. Tamura R, Tanaka T, Miyake K, Yoshida K, Sasaki H (2017) Bevacizumab for malignant gliomas: current indications, mechanisms of action and resistance, and markers of response. Brain Tumor Pathol 34(2):62–77. 10.1007/s10014-017-0284-x. Epub 2017 Apr 6. PMID: 28386777
29. Weijie S (2024) Annexin A2: the feasibility of being a therapeutic target associated with cancer metastasis and drug resistance in cancer microenvironment. Discov Oncol 15(1):783. 10.1007/s12672-024-01693-8. PMID: 39692932; PMCID: PMC11655786
30. Ma K, Chen X, Liu W et al (2021) ANXA2 is correlated with the molecular features and clinical prognosis of glioma, and acts as a potential marker of immunosuppression. Sci Rep 11(1):20839. 10.1038/s41598-021-00366-8. PMID: 34675316; PMCID: PMC8531374
31. Song YX, Li X, Nie SD et al (2023) Extracellular vesicles released by glioma cells are decorated by Annexin A2 allowing for cellular uptake via heparan sulfate. Cancer Gene Ther 30(8):1156–1166. 10.1038/s41417-023-00627-w. Epub 2023 May 25. PMID: 37231059
32. Liu ZL, Chen HH, Zheng LL, Sun LP, Shi L (2023) Angiogenic signaling pathways and anti-angiogenic therapy for cancer. Signal Transduct Target Ther 8(1):198. 10.1038/s41392-023-01460-1. PMID: 37169756; PMCID: PMC10175505
33. Zhai H, Acharya S, Gravanis I et al (2011) Annexin A2 promotes glioma cell invasion and tumor progression. J Neurosci 31(40):14346–14360 PMID: 21976520; PMCID: PMC3201988
34. Huang B, Deora AB, He KL et al (2011) Hypoxia-inducible factor-1 drives annexin A2 system-mediated perivascular fibrin clearance in oxygen-induced retinopathy in mice. Blood 118(10):2918–2929. 10.1182/blood-2011-03-341214. Epub 2011 Jul 25. PMID: 21788340; PMCID: PMC3172807
35. Matsumoto Y, Ichikawa T, Kurozumi K et al (2020) Annexin A2-STAT3-Oncostatin M receptor axis drives phenotypic and mesenchymal changes in glioblastoma. Acta Neuropathol Commun 8(1):42. 10.1186/s40478-020-00916-7. PMID: 32248843; PMCID: PMC7132881

Tables

Table 1 is available in the Supplementary Files section.

Figures

Fig.1 Clinical treatment/research flow and classification

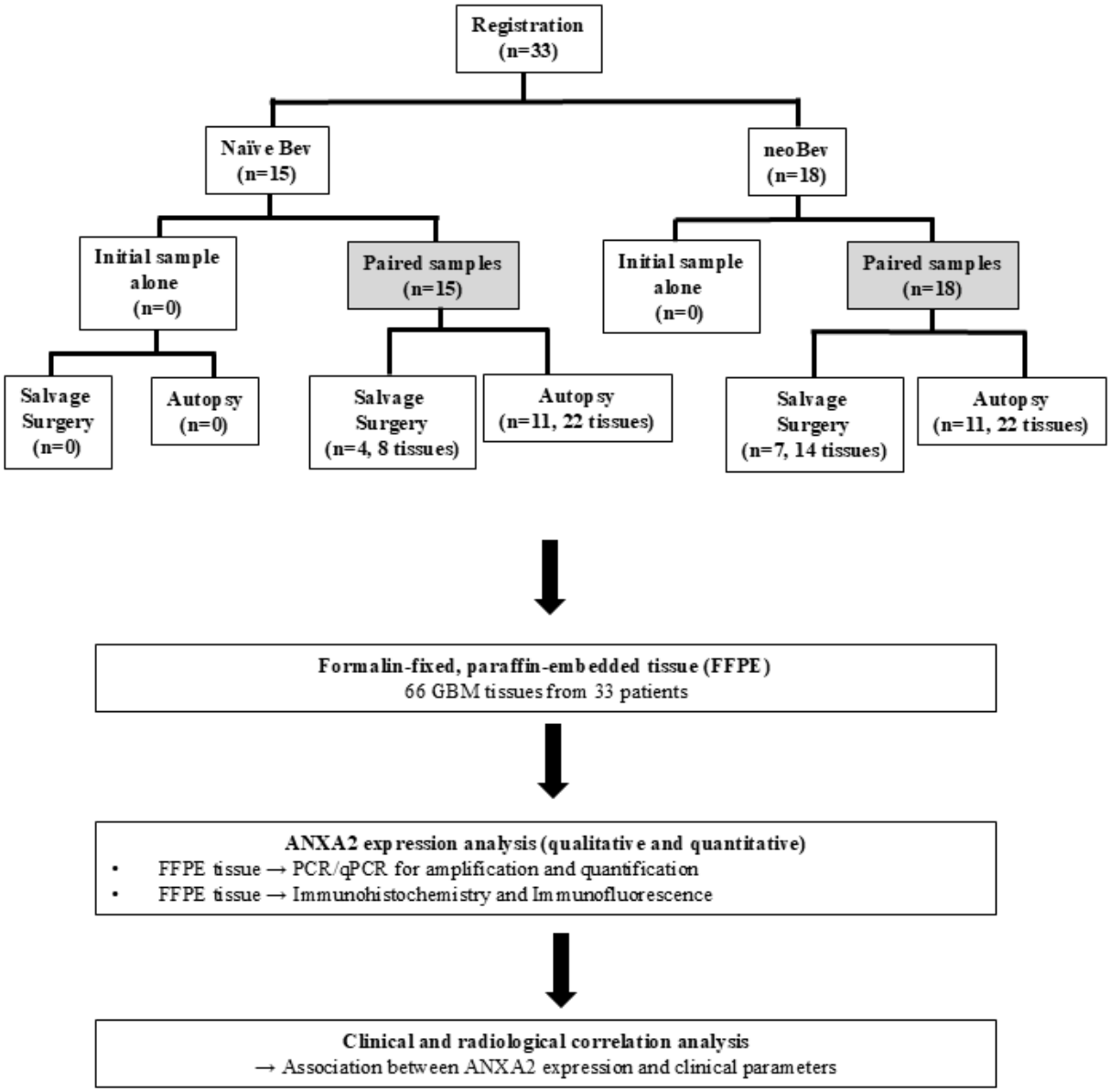


Figure 1

Clinical treatment/research flow and classification of glioblastoma (GBM) samples.

Tissue sampling flowchart for this study. A total of 66 tumor tissue specimens were obtained from 33 patients across three clinical settings: 15 tissues resected before bevacizumab (Bev) therapy (Naïve Bev group), 18 tissues resected under neoadjuvant Bev therapy (neoBev group), and recurrent tumors after

Bev failure (refractory Bev group). For the refractory samples, 22 tissues (8 from the naïve Bev cohort and 14 from the neoBev cohort) were obtained via salvage surgery, while 44 tissues (22 from the naïve Bev cohort and 22 from the neoBev cohort) were obtained via autopsy.

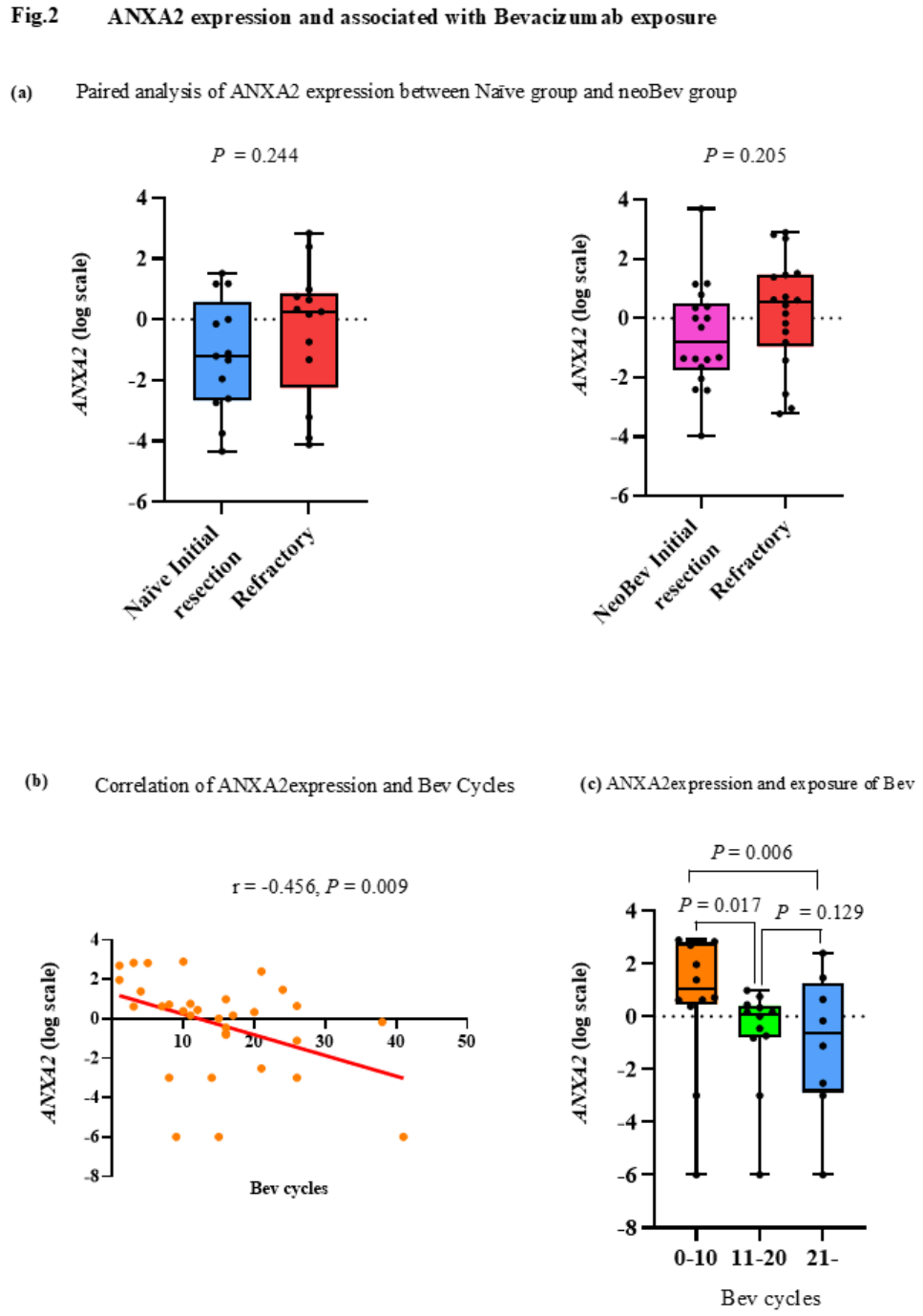


Figure 2

Changes in Annexin A2 (ANXA2) expression associated with bevacizumab (Bev) exposure.
(A) Relative ANXA2 mRNA expression levels were compared using paired tumor samples from patients in the naïve Bev group (n = 15) and those who received preoperative neoBev (n = 18), each paired with corresponding refractory glioblastoma samples. The y-axis represents the $\log_{10}$-transformed relative expression ($\log_{10}$ RE) values obtained from the qRT-PCR analysis. The bars indicate the mean ± standard error of the mean. Statistical significance was assessed using the Wilcoxon signed-rank test. (B) With or without grouping by neoBev, the correlation between the $\log_{10}$ RE ANXA2 expression levels and total Bev administration cycles was assessed using Spearman's rank correlation. (C) The three groups were divided based on the number of Bev administration cycles (0–10, 11–20, ≥ 21 cycles) using the Kruskal-Wallis test followed by Dunn's post hoc test. The y-axis represents the $\log_{10}$ RE levels obtained from the qRT-PCR analysis.

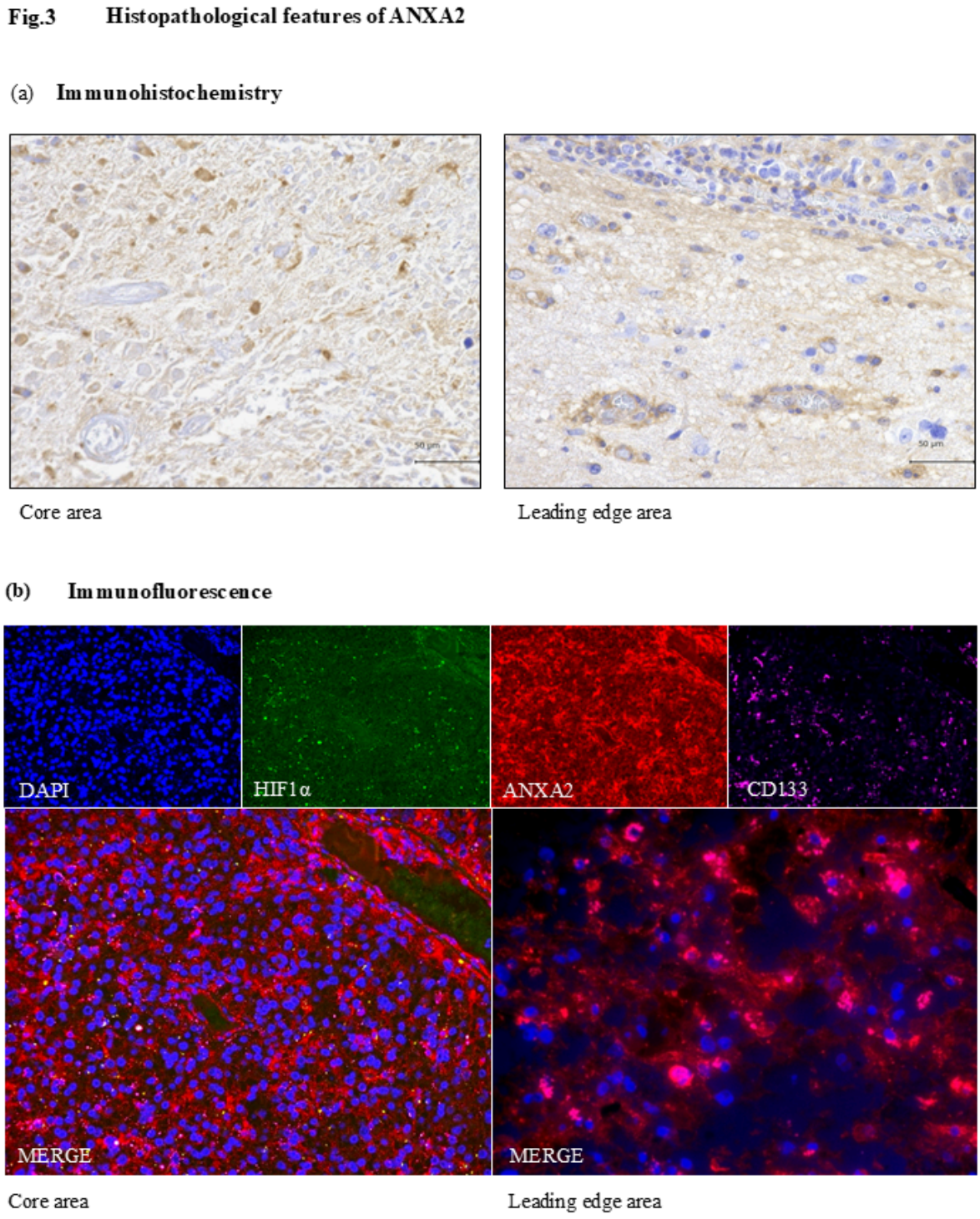


Figure 3

Immunohistochemistry (IHC) and immunofluorescence (IF) assays.

(a) The tumor core and leading-edge area was selected under high-power observational fields at 400× magnification. IHC staining revealed ANXA2 expression in neoplastic glial cells and the stroma, with particularly prominent cytoplasmic staining in vascular endothelial cells at the leading edge. (b) Triple-

label IF was performed to evaluate the spatial distribution of Annexin A2 (ANXA2), hypoxia-inducible factor (HIF)-1α, and CD133 protein expression. Representative IF images showing the sub-cellular localization of these markers, with the nuclei counterstained with DAPI (blue). ANXA2 was primarily localized in the cytoplasm and stroma, whereas HIF-1α showed a nuclear staining pattern. CD133 was predominantly localized to the cell membrane.

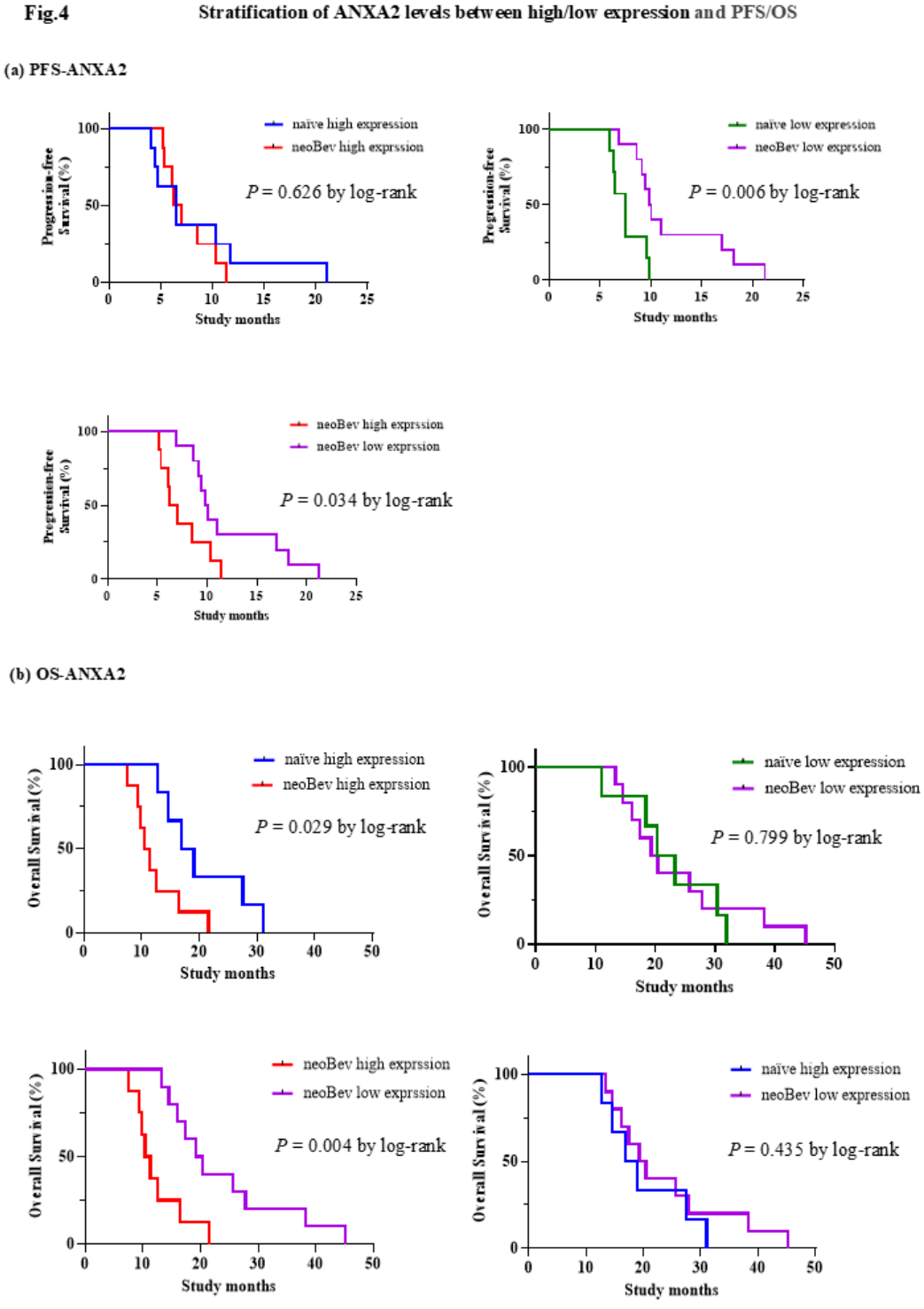


Figure 4

Annexin A2 (ANXA2) expression as a prognostic biomarker in glioblastoma (GBM).

GBM patients were stratified into four distinct subgroups using the treatment option and ANXA2 expression levels at initial diagnosis, defined as follows: 1) naïve low expression, naïve Bev with low ANXA2 expression; 2) naïve high expression, naïve Bev with high ANXA2 expression; 3) neoBev low expression, neoBev treatment with low ANXA2 expression; and 4) neoBev high expression, neoBev treatment with high ANXA2 expression. (a) Kaplan-Meier analysis of progression-free survival (PFS) was performed according to ANXA2 expression patterns, stratified into high and low expression groups relative to the median value. (b) Kaplan-Meier analysis of overall survival (OS) was performed according to ANXA2 expression patterns, stratified into high and low expression groups relative to the median value.

Fig. 5 Pattern of change in ANXA2 during Bev therapy

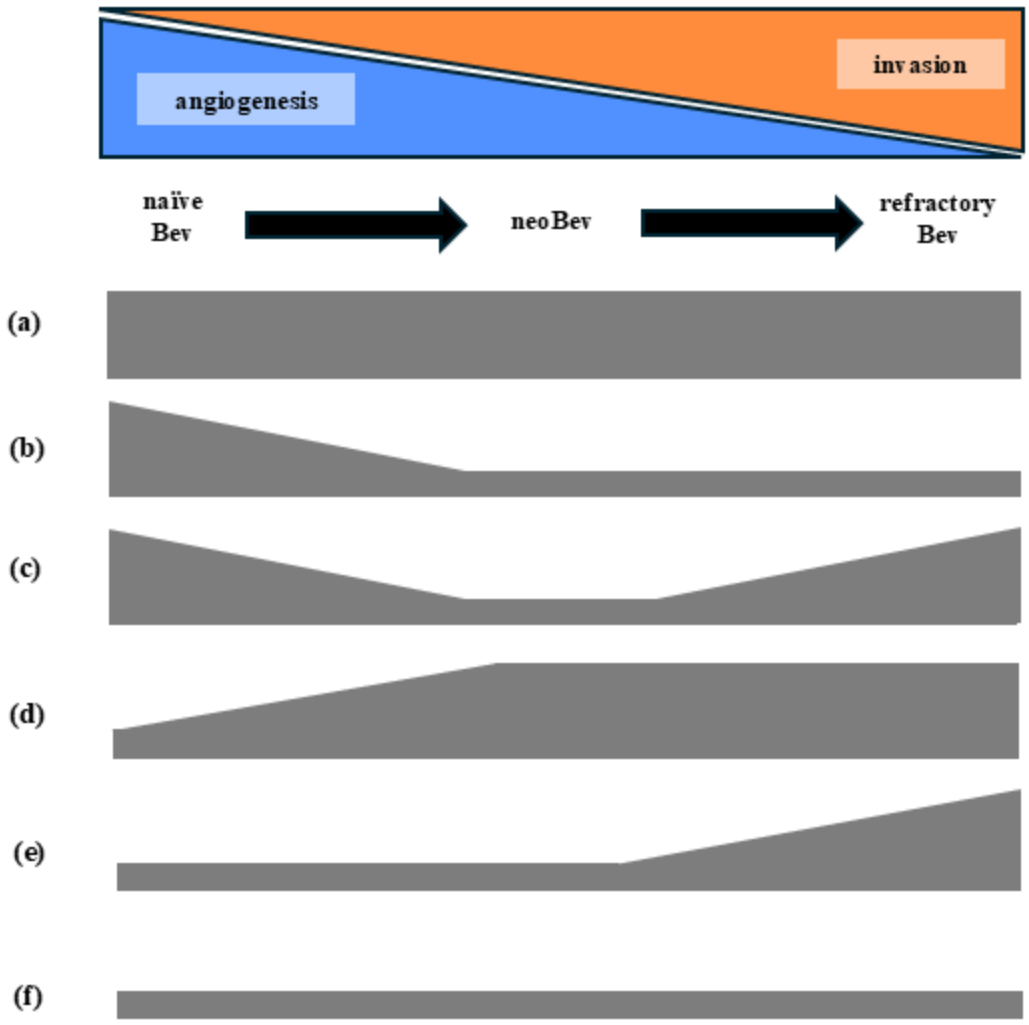


Figure 5

Pattern of Annexin A2 (ANXA2) expression changes during bevacizumab (Bev) therapy in glioblastoma (GBM).

(a) ANXA2-associated poor response: highly angiogenic and highly invasive from the initial stage to the refractory stage.

(b) Favorable response to neoBev with persistent effect t: highly angiogenic at the initial stage and less invasive GBM after neoBev.

(c) Favorable response to neoBev with transient effect: highly angiogenic at the initial stage and less invasive GBM transiently after neoBev.

(d) ANXA2-mediated resistance during neoBev: less angiogenic and less invasive GBM at the initial stage, but Bev-induced invasion observed with neoBev.

(e) ANXA2-mediated resistance during repeated Bev therapy: less angiogenic and less invasive GBM at the initial stage, but Bev-induced invasion observed after repeated Bev therapy.

(f) Favorable response to neoBev with persistent effect: less angiogenic and less invasive GBM from the initial stage to the refractory stage.

Supplementary Files

This is a list of supplementary files associated with this preprint. Click to download.

- Table260617.docx
- SI.Table260617.pdf
- SI.Figure260617.pdf